An Integrated Evaluation of the National Water Model (NWM) Height Above Nearest Drainage (HAND) Flood Mapping Methodology

J. Michael Johnson[1]*, Dinuke Munasinghe[2], Damilola Eyelade[1], Sagy Cohen[2]

[1]University of California, Santa Barbara, Santa Barbara, 93106, USA
[2]University of Alabama, Tuscaloosa, AL 35487

Correspondence to: J. Michael Johnson (jmj00@ucsb.edu)

Abstract. Flood maps are needed for emergency response, research, and planning. The Height Above Nearest Drainage (HAND) technique is a low-complexity, terrain-based approach for inundation mapping using elevation data, discharge-height relationships, and streamflow inputs. The recent operational capacities of the NOAA National Water Model (NWM) and pre-processed HAND products from the University of Texas offer an operational framework for real-time and forecast flood guidance across the United States. In this study, we evaluate the NWM-HAND approach using 28 remotely sensed inundation maps and 54 NHD catchments. The results show the NWM-HAND method tends to underpredict inundated cells in lower order reaches (Strahler order <4) and does better with a slight tendency to over predict, in high order reaches. An evaluation of the roughness coefficient used in the derivation of synthetic rating curves suggests it is the most important parameter for improvement in correcting these errors. Persistent inaccuracies do occur when the NWM streamflow predictions are substantially biased (>60% mean absolute error between NWM and observed streamflow) and in regions of low relief. While NWM values are taken as input, suggestions for handling areas of low relief are provided. Overall, the NWM-HAND method does not accurately capture inundated cells (~20%) but is quite capable of highlight regions likely to be at risk in fourth order streams and higher. While NWM-HAND should be used with caution when identify flood boundary lines or making decisions predicated of whether a cell is dry or wet, its applicability as a high-level guidance tool along larger rivers is noteworthy.

1. Introduction

Floods are one of the deadliest natural hazards in the United States. Over the last 30 years, floods have killed, on average, 86 people annually, increasing in the last 10 years to 95, and between 2015 and 2017 to more than 100 (Lam, 2018). While floods used to be associated with coastal zones, 8 of the 10 US states with the largest flooding disasters in the last decade were landlocked (Lightbody and Tompkins, 2018). Such patterns can be expected to continue as climate and land use pressures amplify (Hirabayashi et al., 2013; Yin et al., 2018). While flood damage cannot be eliminated, it can be mitigated. This is particularly true when populations are given advanced warning, have faith in the forecast accuracy, and are provided actionable intelligence (Johnson et. al 2016, 2018). When emergency responders are given maps showing where water is and where it

might be in the future, better choices can be made that systematically save time, energy, and resources (National Research Council, 2009). Combined, these challenges suggest a need to better understand and forecast flood events across the country.

To convey flood risk, flood maps are used to help stakeholders and the general public better understand and manage risk (Henstra et al., 2019; Merz et al., 2007). Most often these are static maps representing a pre-set event or risk level (e.g. FEMA 100-year flood zones) (Maidment, 2009). Maps that communicate conditions in real-time are becoming more relevant as the severity and socioeconomic fallout of the floods have increased, and technological advances facilitate such forecasts across large domains. While both types of maps require high levels of accuracy, the latter is able to sacrifice some accuracy for gains in forecast domain and speed of delivery.

Since 2015, efforts towards producing real-time and future inundation forecasts for US have resulted in the compilation of a 10m resolution Height Above Nearest Drainage (HAND) layer for the Continental United States (CONUS: Liu et al., 2018). The methodology for coupling streamflow predictions from the National Water Model (NWM) and HAND was initiated as part of the National Flood Interoperability Experiment (NFIE) (Maidment, 2016). The methodology has since been enhanced and added to the National (NWC) US flood forecasting framework (NOAA National Water Center, 2018). The current objective of the NWM-HAND approach is rapid flood inundation prediction for the purposes of disaster warning and guidance. Model accuracy should therefore be viewed in this context and expectations should be tempered while recognizing the importance of having an operational, continental scale flood forecasting system.

A number of studies have shown that the HAND methodology can produce accurate inundation maps from a known streamflow and carefully created HAND layers (Afshari et al., 2018; Rennó et al., 2008; Rodda, 2005; Zheng et al., 2018). There has not been, however, an exploration of how errors in the methodology and its individual components may compound and propagate through the coupled NWM-HAND implementation. In this paper we evaluate the integrated skill of NWM-HAND by comparing simulated events against an observational dataset.

2. Background

To assess the accuracy of the NWM-HAND methodology, inundation maps were created for 28 floodplains across CONUS and compared to an observational flood map repository. Each product used in this analysis is described below.

2.1 Height-Above-Nearest-Drainage (HAND) Method

As the name implies, a Height Above Nearest Drainage (HAND) map contains the vertical distance between a location (grid-cell) and its nearest stream reach. Producing a HAND map requires a terrain dataset and a spatial representation of a region's river network to define local drainages. In the USA these primarily come from the USGS National Elevation and Hydrography

Datasets respectively (NED and NHD). For the context of this study, all references to the NHD refer to the medium resolution dataset unless otherwise stated. Each polyline in the NHD is described as a 'reach' and assigned a unique common identifier (COMID). To calculate the 'nearest drainage', the contributing catchment for each reach is rasterized to the spatial resolution of the DEM. To illustrate this, a generic catchment (reach 101) is shown in Figure 1A. In this example, all cells in the catchment inherit the COMID (101) associated with the draining reach (Figure 1B).

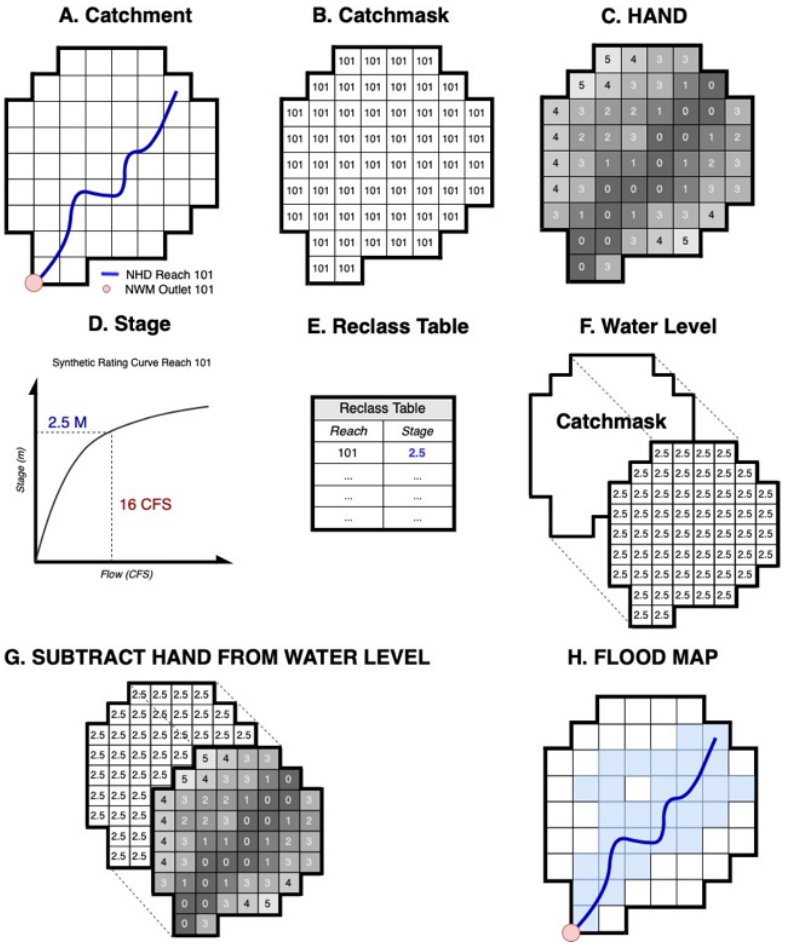

Figure 1: The HAND methodological workflow: (A) The contributing catchment to a defined outlet is rasterized to the resolution of the supporting DEM (B) This raster is reclassified to match the identifying code of the outlet. (C) In and out-of-stream cells are identified using the flowline vector. The relief between all out-of-stream cells from their nearest in-stream-cell is calculated to define a HAND raster. (D) From a given flow rate, a rating curve can be used to convert flow to stage. (E) A reclassification table can be built relating the reach COMID to the current

stage. (F) The table can then be used to reclassify the catchmask, into a water-leve rasterl. (G) Subtracting C from F yields a water-level above surface raster. All values less than 0 can be set to 0 and the remaining show the estimated flood height at each cell (H).

To generate a HAND raster, a river network is used to determine in-stream and out-of-stream cells. For all out-of-stream cells, the relief between that cell and the nearest in-stream cell is calculated (Figure 1C). In the pre-computed HAND rasters, relief was calculated via the TauDEM distance down function (Tesfa et al., 2011). Once computed, HAND raster's can be used to define hydraulic flood plain cross-sections for all reaches. The derived geometries provide cross sectional areas (A) and hydraulic radius (R) inputs for the Manning's equation (Zheng et al., 2017):

$$Q(y) = \frac{1}{n} \times A \times R^{\frac{2}{3}} \times S^{\frac{1}{2}} \quad (1)$$

where Q(y) is the discharge for a given stage, n is the Manning's roughness coefficient, and S is the reach slope. Reach slope is an attribute of the NHD dataset, while a constant channel roughness (n) of 0.05 has been adopted for synthetic rating curve (SRC) generation (Zheng et al., 2018, Johnson and Coll, 2017). From this equation, streamflow requirements for a set number of stage values can be generated (Zheng et al., 2017). Finally, subtracting a HAND raster from a water-level raster yields a water height raster (Figure 1G). where any value greater than zero is classified as flood and values less than zero indicate dry cells (Figure 1H).

In 2017, HAND raster's and SRCs were generated for CONUS using the 10-meter NED and NHD datasets on the ROGER supercomputing system at the University of Illinois Urbana Champaign (Liu et al., 2018; Zheng et al., 2017). All products are catalogued by HUC6 (the basin level units in the WBD) on the UT Corral Server. (https://web.corral.tacc.utexas.edu/nfiedata/).

2.2 National Water Model (NWM)

The NWM serves as a cornerstone of the new NOAA Water Initiative to provide integrated predictive capabilities that promote resilience and mitigation of water risks (Cline and Maidment, n.d.). In August 2016, version 1.0 was made operational, expanding the Nation's forecasting domain from approximately 9,000 forecasting locations to 2.7 million reach outlets along the NHD. At each of these points the NWM generates hourly streamflow forecasts and 1-km forecasts of soil moisture, runoff, snow water equivalent, and other water balance states.

The core of the NWM is the WRF-Hydro modelling architecture supported by the National Center for Atmospheric Research (NCAR) (Gochis et al., 2018). The NWM routes water over the NHD, producing streamflow values at the end point of each reach (indexed by COMID (Figure1A – pink dot)). The NWM runs in four configurations: analysis and assimilation, short

range, medium range, and long range (NOAA, 2016a; 2016b; Salas et al., 2017). The analysis and assimilation configuration assimilates observed streamflow data from the USGS NWIS network and provides an hourly snapshots of current hydrologic conditions out to three hours. The short-range configuration produces hourly deterministic streamflow and hydrologic state forecasts 18 hours out; the medium range configuration produces 3-hourly forecasts out to 10 days; and the long-range configuration generates a 30-day, four-member forecast ensemble (NOAA, 2016a).

Operational data is publicly available for a 48-hour rolling window on the NOAA NOMADs server and can be accessed directly or through a number of user-contributed packages and end-points (Johnson, 2018a). In addition to the operational products, 23-year reanalysis studies have been run for NWM versions 1.0, 1.2, and now 2.0. These products use downscaled NLDAS-2 climate forcing's with Noah-MP, a groundwater bucket model, overland and subsurface routing, and NHDplus channel routing. Unlike the operational Analysis and Assimilation (A&A) products, the reanalysis simulations do not assimilate USGS streamflow data and have been calibrated in limited number of basins (Gochis et al., 2016). In this study, the v1.2 reanalysis product was accessed through Amazon Web Services (https://registry.opendata.aws/nwm-archive/).

2.3 U.S. Flood Inundation Map Repository (USFIMR)

Following the release of the NWM, academic partners at the University of Alabama developed the US Flood Inundation Map Repository (USFIMR) to provide inundation maps for past U.S. flood events. These maps were derived by image classification techniques from a number of satellite sensors (e.g. Landsat, Sentinel-1, 2) with some ground truthing based on secondary sources (e.g. news reports, social media). Such maps are useful for model calibration, validation, and flood susceptibility assessment (Cohen et al., 2018; Munasinghe et al., 2018). The USFIMR web portal provides more information on each flood, the specific sensor, as well as supplementary data including NED elevation and upstream NWIS hyperlinks (http://sdml.ua.edu/usfimr). A catalogue of the USFIMR maps used in this study can be found in the appendix table 1. Here it is noted that the FloodID assigned to each flood in this analysis is consistent with those used in the USFIMR and not fully sequential.

3. Methods

For each USFIMR map, the AOI and HydroData R packages were used to determine the minimum bounding box of each floodplain and subset the NHD (Johnson, 2018a, Johnson, 2018b). A list of COMIDs and HUC6 identifiers were extracted from the NHD attributes. For each HUC6, the HAND, catchment and rating curve products were downloaded cropped and, when necessary, mosaicked. The timestamp of each USFIMR satellite image was used to query the needed NWM v1.2 reanalysis values and generate an inundation map. This process was repeated for each USFIMR flood map and the process is formalized in the Flood Mapping R package (Johnson, 2019).

To facilitate comparison, the USFIMR shapefiles were projected from NAD83 / Conus Albers (CRS 5070) to a WGS84 coordinate reference system (CRS 4269). For each shapefile, a clipping extent, derived as a concave hull was created to ensure that all pixels being evaluated were within the USFIMR classification bounds. A waterbody mask was created by combining the perennial NHD water bodies (NHD Fcode 39004, 39009) and NHDAreas (NHD FCode 40300, 40307, 40308, 40309) in each extent. The USFIMR flood, extent, and waterbody mask, were all rasterized to the 10m HAND grid using the fasterize R package (Ross, 2018). All cells that were not within the concave hull or covered by a waterbody mask, were set to NA prior to comparison.

After processing, grid-cells in the simulated and observed maps for each case study were intersected and classified into four categories seen in Table 1. In these categories, 'W' refers to a wet cell and 'D' refers to a dry cell. The first letter in each category refers to the state of the cell in the USFIMR map while the second refers to the state of the cell in the NWM-HAND simulation. With this classification, four metrics were established to describe the area ratio, and rate of accuracy, overprediction and underprediction. The last three of these are derivatives of the fit statistic used by Sangwan and Merwade (2015).

Table 1: Flood Comparison Confusion Matrix.

	Modeled Wet	**Modeled Dry**
Observed Wet	*WW (true wet)*	*WD (false dry)*
Observed Dry	*DW (false wet)*	*DD (true dry)*

The spatially-agnostic Area-Ratio helps establish if the NWM-HAND method is inundating the correct number of cells regardless of spatial accuracy. Any value less than one indicates the NWM-HAND method is not inundating enough cells while a value greater than 1 indicates too many cells were inundated.

$$AreaRatio = \frac{Total\ Wet\ Simulation\ Cells}{Total\ Wet\ Observed\ Cells} \quad (2)$$

Overall Accuracy is quantified as the number of cells that were correctly identified as wet (WW) divided the number of all wet cells in the simulated and observed rasters:

$$Accurate\ (A) = \frac{WW}{WW+WD+DW} \quad (3)$$

Similarly, areas of Underprediction are quantified as:

$$Under\ (U) = \frac{WD}{WW+WD+DW} \quad (4)$$

And areas of Overprediction as:

$$Over\ (O) = \frac{DW}{WW+WD+DW} \quad (5)$$

The use of a common denominator assures the summation of Over, Under and Accurate equals 1, and collectively these values form the Accurate, Over and Underpredict (AOU) metrics. The choice of a 2D fitness statistic (examining only the extent of flood, as opposed to depth and timing of flood propagation) is governed by the aerial imagery products available (which only captures the extent of the flood, at a singular point in time). By electing this form of evaluation, we only analyze the strengths of NWM-HAND simulations at the given time-step coinciding with the time of image capture (not necessarily peak flooding).

In this paper we are also interested in isolating the biases stemming from NWM streamflow forecasts and from issues with HAND/SRC layers. To do this, we collected all USGS National Water Information System (NWIS) gages within the minimum bounding box of each USFIMR case study. For each NWIS gage, the collocated COMID was identified using the Network Linked Data Index (HydroData binding). To be kept in our analysis, each catchment had to have an NWIS and NWM record for the date/hour of interest; (2) the complete catchment had to be contained within the USFIMR concave hull and; (3) a flood needed observed in that catchment within the USFIMR map. Streamflow values from the NWIS and NWM were compared using a normalized mean error (nME) and normalized mean absolute error statistic (nMAE):

$$nME = \frac{Q_{NWIS} - Q_{NWM}}{Q_{NWIS}} \quad (6)$$

$$nMAE = \frac{ABS(Q_{NWIS} - Q_{NWM})}{Q_{NWIS}} \quad (7)$$

In total, these filters yielded 54 unique catchments within the 28 USFIMR floodplains for which NWM-HAND and NWIS-HAND inundation maps and AOU metrics were generated.

The changes between the NWIS and NWM-driven flood maps were calculated as the standardized difference in the accuracy (A) metric of each (equation 8). Equation 8 utilizes the percentage-based properties of the accuracy metric to describe the normalized level of change experienced by using known streamflow values. Positive values indicate the use of NWIS data increased the accuracy of the produced flood map while negative values indicate the use of NWIS decreased overall accuracy.

$$\Delta A = \frac{A_{NWIS} - A_{NWM}}{A_{NWIS}} \quad (8)$$

4. Results

4.1 Area Comparison

First, we evaluate the ability of the NWM-HAND method to produce the correct amount of inundated area. Area ratios (Eq. 2) are shown in Figure 2.

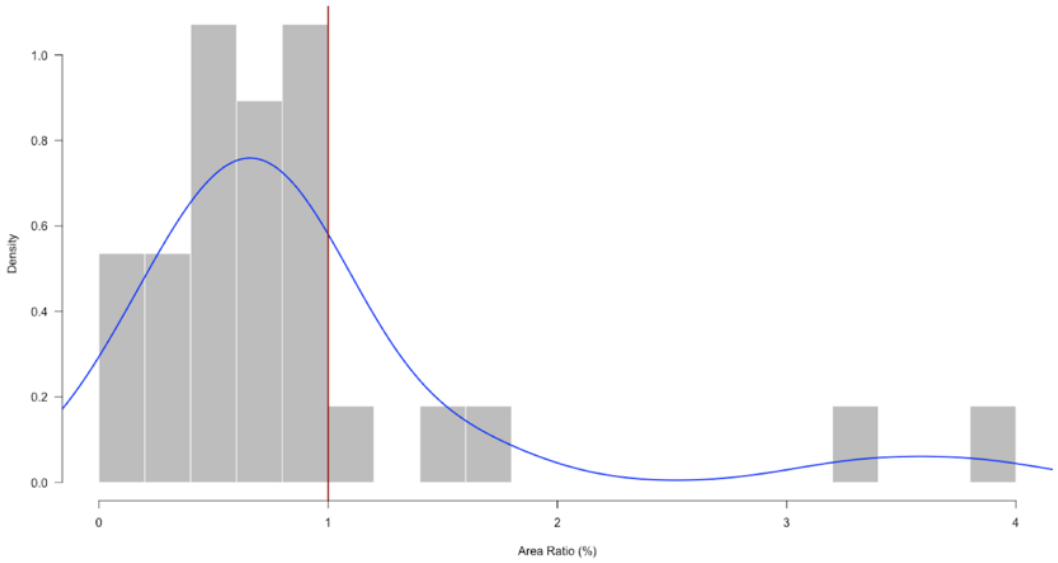

Figure 2: A histogram of area-ratios for our 28 floodplains show a tendency for the NWM to underpredict flood extents.

Figure 2 shows that 82% of the case studies had an area ratio less than one. Of the under predicting cases, the average area-ratio was 60% (40% underprediction in area). The overall median of the sample was 73%, with an Inter Quartile Range (IQR) of 47-96%. While there are fewer cases of total-area over prediction (5), the instances tend to be large with a mean of 230.4%. This suggests that in all but the extreme cases, inundated areas are underrepresented.

From a spatially explicit perspective we evaluated how the NWM-HAND approach captures cell-level inundation. Figure 3 shows the AOU metrics for each flood as a stacked bar-plot.

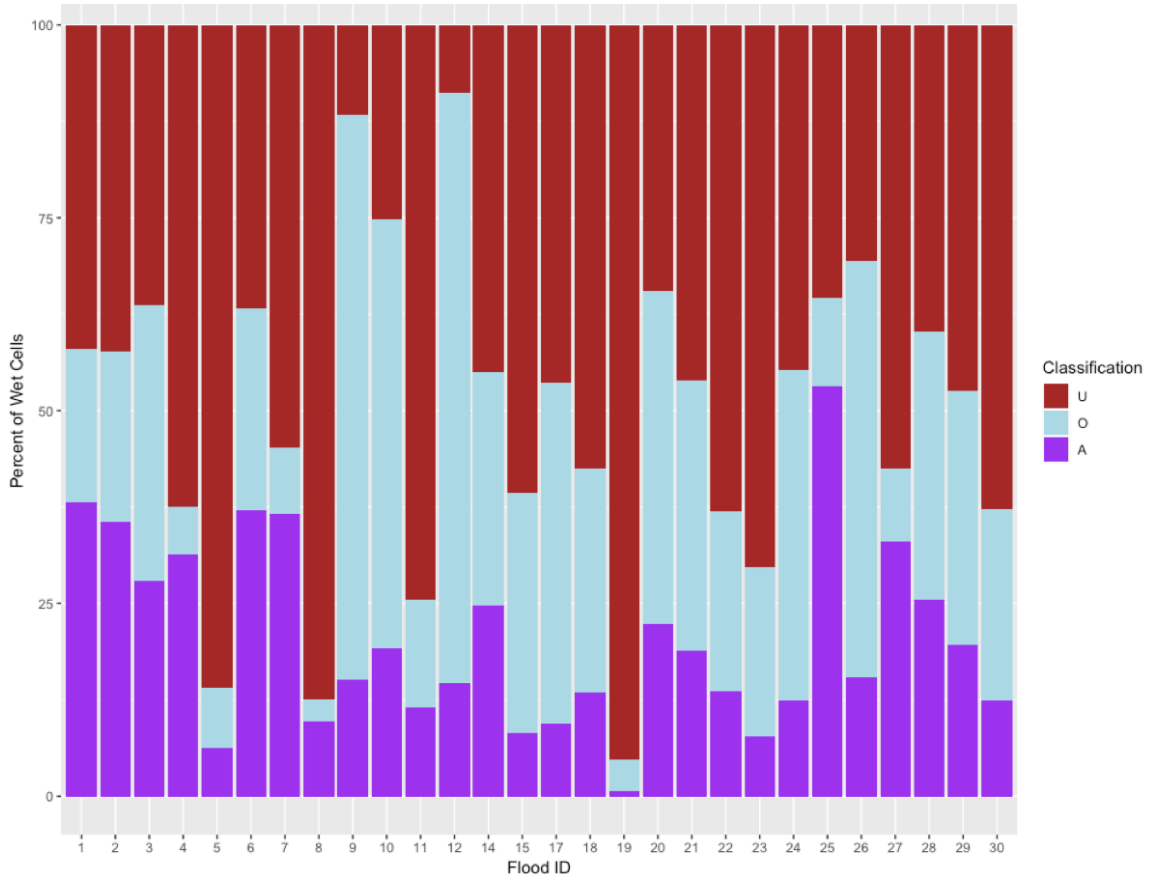

Figure 3: Stacked bar plot of the Accuracy, Over, and Under predict (AOU) metrics for each case study. Each bar represented 100% of the inundated cells in the intersected simulation and observed case study and the percentage of cells that were accurate, over and under predicated.

Figure 3 emphasizes the tendency towards underprediction (maroon) across our case studies. Table 2 shows that, of all flooded cells (in either the simulation or observed data), 37 - 63% (IQR) fall within the under predicted category, 10 - 36% (IQR) were overpredicted and 10-27% (IQR) are correctly identified with a mean of 19%.

Table 2: Summary statistics across the 28 case studies.

	Min	1st Quartile	Median	Mean	3rd Quartile	Max
Accurate	0	0.10	0.15	0.19	0.27	0.53
Over	0	0.10	0.25	0.27	0.36	0.76
Under	0.09	0.37	0.47	0.53	0.63	1.0

These statistics show a clear signal that the NWM-HAND method is limited in its ability to capture inundation and is almost twice as likely to underpredict than overpredicted the status of a missed cell. Noting the stated intention of NWM-HAND is creating an operational flood mapping framework for emergency guidance, this tendency raises concerns. These results indicate there is significant room for improvement in the NWM-HAND inputs but making these improvements requires a better understanding of the largest sources of error. In the following sections we more closely explore the 54 gaged catchments to better understand the influences driving performance.

4.2 Catchment Area Comparison

To evaluate the influence of NWM uncertainties on the inundation, summary statistics for the NWM and NWIS-driven AOU metrics are presented in Table 3.

Table 3: IQR and mean values for NWM-NWIS flow comparisons and inundation metrics for 54 NHD catchments.

	1st quartile A_{NWM} / A_{NWIS}	Median A_{NWM} / A_{NWIS}	Mean A_{NWM} / A_{NWIS}	3rd quartile A_{NWM} / A_{NWIS}
Accurate	9% / 9%	16% /16%	25% / 25%	38% / 43%
Over	17% / 23%	45% /47%	44% / 47%	66% / 70%
Under	4% / 3%	26% / 21%	31% / 28%	53% / 46%

Table 3 highlights that using known streamflow values generates minimal changes in average accuracy except in the upper quartiles. In a broad sense, the influence of NWM streamflow appears small (e.g. ±3%) under average conditions increasing to about ±6% on the outer quartiles. This indicates that either the NWM is preforming well at these stations or the NWM-HAND model is robust to errors in NWM input.

A linear regression between each NWM and NWIS AOU metric shows R^2 values of 93%, 82%, and 75% respectively. This means that approximately 7% of the variation seen in accurate prediction can be attributed to inaccuracies in the NWM forecasts, as well as 18% of the variation in over prediction and 25% of the variation in underprediction. Given the nME of the NWM forecasts throughout our catchment sample was -20% (IQR (-55)-5%), the relative order of NWM influences seem correct, while highlighting the generally small influence in overall attribution. Table 3 also indicates that, using both NWM and NWIS streamflow, the tendency at the catchment level is to over predict (NWM 17-66% IQR) rather than under predict (4-53%) inundation. This is a opposite pattern seen when looking at the entire floodplain maps.

4.3 Influences of NWM streamflow inputs

Of our 54 samples, the NWM produces a nMAE of 20% or less in 37% of our catchments and an nMAE of 40% or less in 50% of the catchments. Seventeen (17%) of the catchments showed a nMAE greater than 70%, and the average nME was -

20% (IQR -54 – 6%) indicating a general tendency for the NWM to underpredict high flows. To better understand the relative bias introduced by the NWM inputs we grouped our 54 NHD catchments by their nMAE.

Table 4: AOU metrics grouped by nMAE

nMAE range	Gages (cumulative %)	Mean ΔA	Absolute mean ΔA	NWIS mean A / O / U	NWM mean A / O / U
0 - 10%	9 (16.67%)	-0.24	0.68	25 / 47 / 29	25 / 47 / 29
10 - 20%	11 (37%)	1.64	1.91	20 / 61 / 19	20 / 61 / 19
20 - 30%	4 (44%)	3.92	4.18	21 / 36 / 43	21 / 32 / 47
30 - 40%	3 (50%)	-6.36	6.36	30 / 20 / 50	30 / 19 / 51
40 - 50%	3 (55.8%)	-0.3	6.81	38 / 48 / 14	39 / 43 / 18
50 - 60%	6 (66.7%)	-0.55	8.39	47 / 48 / 5	47 / 44 / 9
60 - 70%	8 (81.49%)	4.90	31.77	22 / 50 / 28	20 / 42 / 38
70 - 80%	1 (83.3%)	69.52	69.52	2 / 8 / 90	0 / 3 / 97
80 - 90%	3 (88.90%)	30.15	30.15	22 / 36 / 42	14 / 23 / 63
90 - 100%	2 (92.60%)	3.54	84.36	10 / 67 / 23	13 / 32 / 54
>100%	4 (100%)	-360.51	391.42	12 / 46 / 41	12 / 74 / 14

For each set of basins grouped by nMAE, the number of gages, mean and absolute mean ΔA along with the average AOU metrics for the NWM and NWIS driven maps are shown in Table 4. Looking at the mean absolute error between the NWIS and NWM maps, there is evidence that the influence of the NWM on NWM-HAND accuracies are minimal until nMAE exceeds 60% when there is a clear jump in the absolute mean ΔA from less than a 10% relative loss to more than 30%.

4.3.1 NWM-HAND Errors when nMAE exceeds 60%

When the NWM exceeds nMAE of 60%, predictable patterns of error occur. Figure 4A (Flood ID 4), shows a case where NWM-HAND under predicts inundation due to an underpredicted NWM forecast. Figure 4B (Flood ID 9) shows a case where an over predicted NWM forecast results in over predicted flood extents.

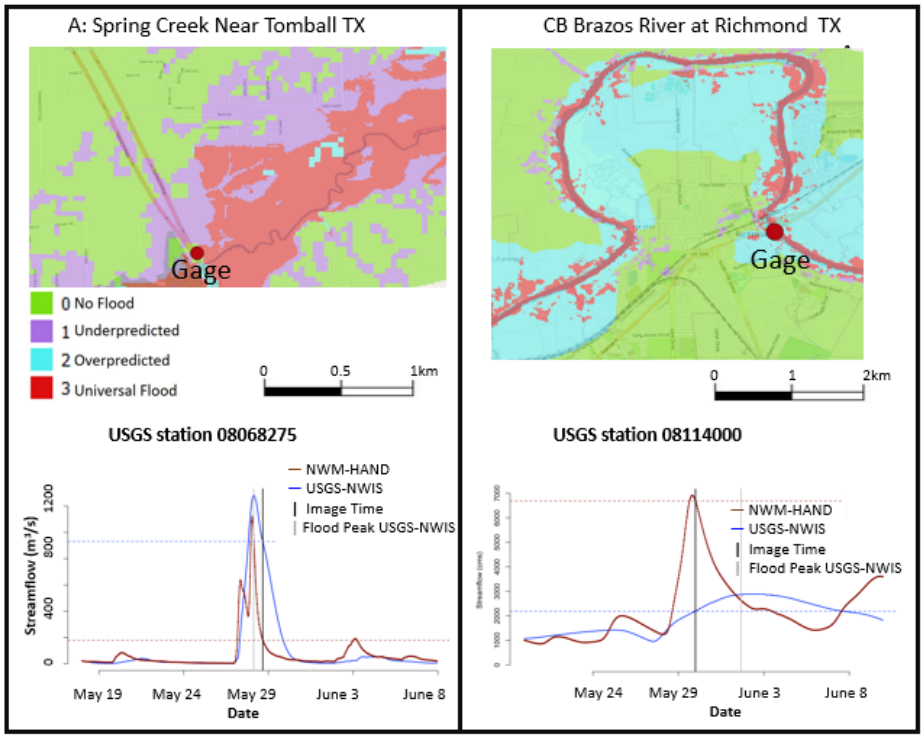

Figure 4: Prediction errors due to NWM flow forecast: (A) NWM underprediction results in underpredicted flood extents. (B NWM overprediction results in overpredicted flood extent.

4.3.2 NWM-HAND Errors when nMAE is less then 60%

Previously we noted that NWM-HAND maps showed minimal deviation from those produced with NWIS values when the NWM was within 60% of the observed streamflow. Also, we noted the catchment sample shows the opposite pattern of the floodplain analysis – errors tend towards over prediction rather than under prediction, despite the average tendencies of the NWM to under predict streamflow (nME of -20%). To visualize this, the area ratios for our 54 catchments are plotted in Figure 5.

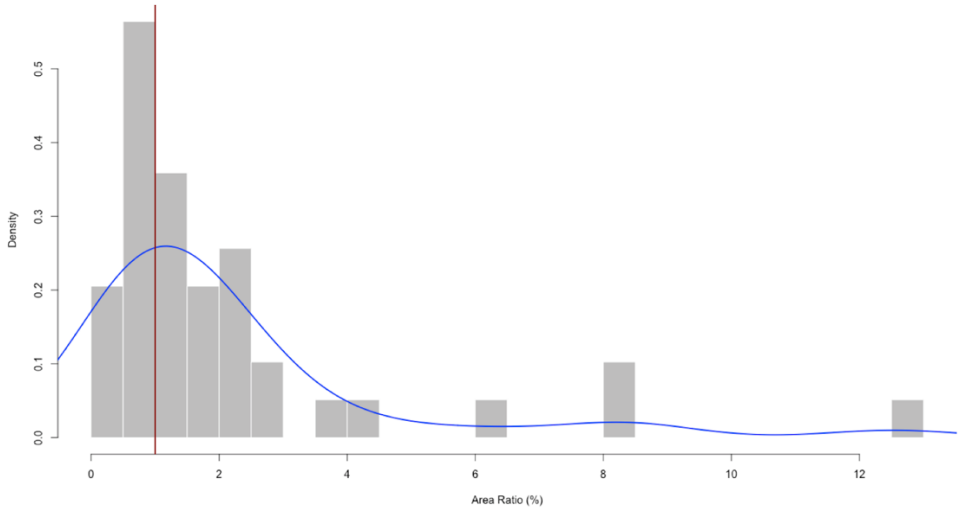

Figure 5: A histogram of area-ratios for 54 catchments show a tendency for the NWM to slightly overpredict flood extents in most cases and a long right tail of extreme over prediction.

When compared to Figure 2 (area-ratios of floodplain case studies) we see the peak in the density curve now sits much closer to 1 with a more equal proportions on either side. This indicates that at the catchment level, NWM-HAND is better able to capture the total area of inundation. However, we see that the over predicted cases are much more extreme causing the right tail to elongate.

Of the 54 catchments, 90% were of a Strahler stream order of 4th or higher. In comparison, when all catchments in each of our USFIMR floodplains were aggregated, low order reaches made up, on average, 81% of the total stream networks. From here on out, lower order reaches refer to those with a Strahler order of 4 or less, and higher order refers to those with a Strahler order or 4 or higher. In many ways, this makes our sample catchments a biased sample favouring high order reaches. Our hypothesis here, is that the difference in patterns seen between the floodplains and catchments can be explained by the difference in the sample and population. That is low order reaches tend to be underpredicted while higher order reaches perform better with a tendency towards over prediction.

4.4 Underprediction in lower order reaches

A visual analysis of our floodplains also reveals a distinct pattern of under prediction in lower order reaches. We illustrate this using the only gaged 2nd order stream in our sample (Fig 6, Flood ID 8 USGS Station ID 8068325). At this reach, the NWM estimated 50 m^3/s flowing through the channel producing a SRC stage of 1.82 m. The recorded NWIS flow is 80 m^3/s (nMAE = 0.38) which would produce an SRC stage of 2.43 m. A cross section was made across the HAND raster for this reach and shows a stage of 3.3 is required to inundate the right bank and 3.8 m is needed to inundate the left bank to the levels seen in the USFIMR.

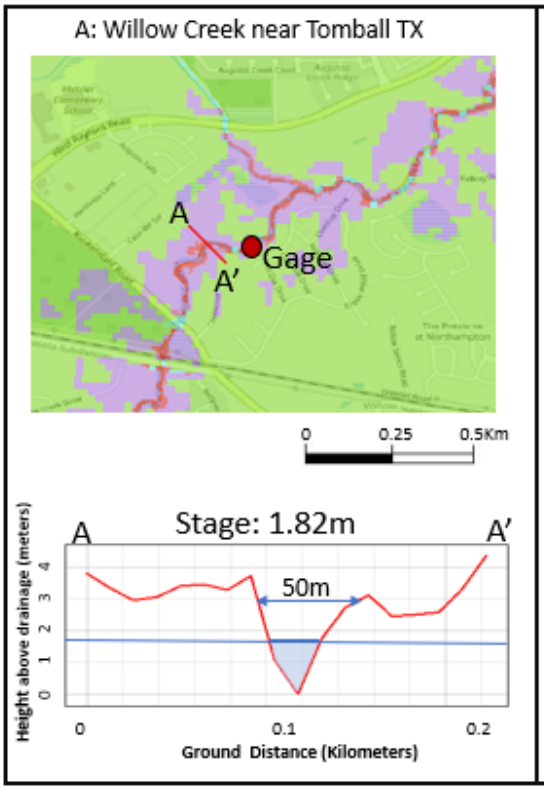

Figure 6: Inaccurate synthetic rating curve relationship causes underprediction in a 2nd order stream

In this case, even if the NWM was able to accurately predict streamflow, water would have remained confined to the channel. Recognizing a mismatch between the known Q (80 m^3/s) and the stage observed in the USFIMR (3.8 m) we explored the assumptions driving the Manning's Equation SRC for this reach (equation 1). Keeping slope (NHD attribute) and the cross-sectional area required to generate a stage of 3.8 m constant, we independently varied the roughness coefficient (n) and the hydraulic radius (via the wetted perimeter), solving for a Q of 80 m^3/s. In doing so we found that the SRC relationships are generally insensitive to changes in hydraulic radius (needed to be increased by a factor of 10), but were sensitive to changes in Manning's n. Specifically, we found that an N of 0.16 was needed to achieve a realistic streamflow-stage relationship at this reach. Based on this representative example we suggest that systematically increasing roughness in lower order reaches may help mitigate underprediction. The literature and other model structures also support such a change. For example, the NWM itself uses n values of 0.06 for first and second order reaches, and 0.055 for third and fourth order reaches. Other projects apply n values by stream order more similar to what we found in our example (n = 0.12 for second order reaches; Li, 2016). More research is needed on the relative role of roughness in the NWM-HAND method and the best way to optimize it across different stream orders and geographies.

4.5 Overprediction in areas of low-relief

Throughout our evaluation, over prediction in low-relief catchments became evident. Moreover, such catchments account for the majority of the long right tail seen in Figure 5. We found two type of cross-sections occurring in areas of low relief, ones that are very sensitive to errors in stage, and, ones that are fundamentally limited by the terrain representation in the HAND layer. Since HAND is not a physical model, it is unable to conserve volume through space or time. In areas of low relief, where many cells have similar if not equal HAND values, small errors in stage can have disproportionate errors in inundation extent at the 10m grid cell resolution. The Washita river at Anadarko OK case study (Figure 7A) shows a 6-order stream with low relief. The NWM estimates 473 m^3/s producing and SRC stage of 3.81 m. Comparatively, the recorded flow was 495 m^3/s producing an SRC stage of 3.88 m. The nMAE of 4% suggests the source of overprediction originates in the terrain layer or SRC. A cross-section of this landscape reveals a channel with relatively uniform overbank terrain. For this reach, we optimized the SRC for the cross section at an observed stage of 1.2 solving for a Q of 495 m^3/s. To achieve this, n was reduced to 0.005, effectively increasing the carrying capacity of the river. This solution supports the pattern of decreasing n in higher order rivers and this emphasizes that fact that in areas with low relief, small errors in stage and or discharge can result in extreme overpredictions.

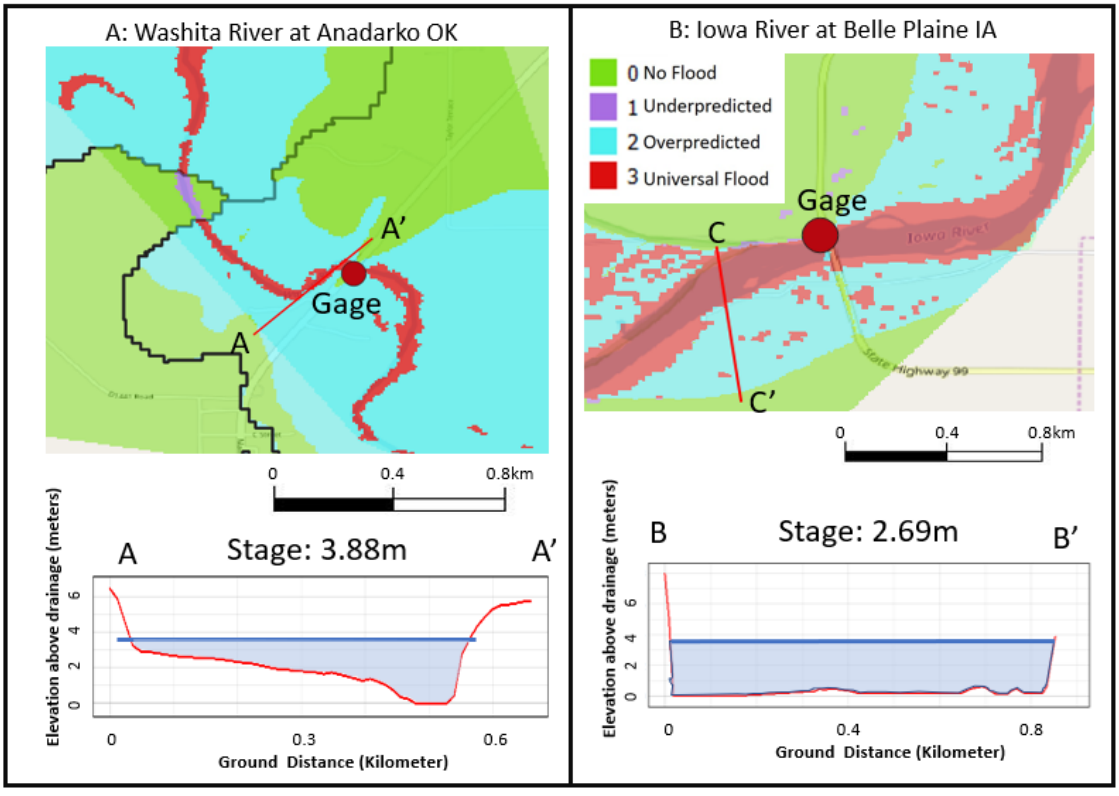

Figure 7: Over prediction in catchments with low relief. (A) This catchment is influenced by a poor synthetic rating curve relationship and highlights the influence small errors in Q/stage can have on inundation (B) This catchment exemplifies a case where the HAND layers will be unable to accurately capture flooding extents due to essentially 0 relief.

We examined a second type of low relief profile where optimizing the hydraulic parameters has no effect due to the form of the HAND raster. This is illustrated with a cross section along the Iowa River at Belle Plaine IA (Figure 7B Flood ID 17). The NWIS observed streamflow for the reach was 971 m^3/s (stage = 2.69 m) while the NWM predicted streamflow was 958 m^3/s (stage = 2.66). The issue with this reach (and others like it) is that the area currently simulated as flooded, will flood for any stage exceeding 0.5 m regardless of the volume of water within the channel. It is in these regions that the 10 m grid cell resolution of the underlaying DEM and absolute vertical accuracy of 2.44 meters (FEMA, 2007) appear most limiting.

We suggest two possible improvements for low relief catchments. The first is refactoring of the NHD catchments (or the effective HAND catchments) into more uniform units avoiding large, flat drainages and instances of many small units. Tools for NHD refactoring are already in development (Blodgett, 2018), and the idea of refactoring speaks to issues to be raised in section 4.6. A second possible alternative to refactoring is to make use of the NWM velocity and flow estimates to define cross sectional areas from the NWM forecast:

$$Cross\ Sectional\ Area = \frac{Q}{Velocity} \tag{9}$$

The intention would be to allow the physical model (NWM) and routing-routines (WRF-Hydro) to deal with issues of volume preservation. The resulting cross-sectional areas could be used as an Area-Stage rather than Q-Stage look up within the existing SRCs. This would work around some of the issues with roughness (outsourcing to the NWM) while capitalizing on the observed accuracies in the floodplain cross sections. Moreover, by controlling for the volume of water in the channel instead of the height, low lying areas will be less prone to exaggeration. Such a change would require (1) an understanding of how the NWM is handling hydraulics and thus velocity and (2) a test of how variations in velocity impact volume estimation. Both are interesting pursuits in their own right but out of scope for this paper.

4.6 Data Models: Use, Limitations, and Adaptions

The Digital Elevation Model (DEM) used to prepare the current HAND layers is a 10 m product that effectively smooths the surface of the earth. In areas of the low relief, higher-resolution elevation data would be able to produce more sensitive rating curves. In other areas, attention to the methods and datasets (streamlines) used to condition the DEM should be considered.

With respect to the streamlines it is important to recognize that the NHD was developed as a cartographic representation of the nation's waterways and using a cartographic toolset for hydrologic modelling and routing applications has inherent limitations. In Figure 8A (Flood ID 12), the NHD does not capture the meandering segment of the Canadian River's main channel. In such a situation, even with accurate NWM forecasts and rating curve relationships, the predicted flood extent will be spatially misaligned. A similar situation can also occur in areas with braided channels or wide estuaries. Standard DEM-based stream delineation tools (used in NHD) only allow one channel to be designated for each reach and often miss small reach cannels (such as 1st and 2nd order reaches). This results in poor representation of the stream network density or channel width and an inability to capture the spatial extent of flooding. Prediction errors due to missing reaches can be seen in FloodID 8, while errors due to channel and or coastal feature representation can be seen in FloodIDs 19, 23 and 24.

On a more theoretical side, the use of a cartographic datasets as model domain-based layers often involves some form of manipulation. Up until this point, the NHD has been used in its original form without considerations for the implications on modelling. As the NHD becomes a more central component of the NWM framework, the goal of creating more specific and consistent modelling units (catchments), while preserving the network is of value. To illustrate an example of this, Figure 8B shows a collection of catchments in FloodID 17. The two principle catchments experiencing flooding in this image are highlighted in red. Both catchments are long and narrow making them inconsistent with the others in the region. Better segmenting the long reaches would allow for smaller catchment units. One issue with these long catchments can be seen in the leftmost red catchment. To the north of the catchment (in the black catchment) we see a large swath of under predicted flooding. Looking at the NHD reach draining the black catchment it is easy to see that the area of missed flooding did not stem from the catchment reach but from the long red catchment. This implies that flood water crossed the catchment boundaries in a way that cannot be captured by HAND. Such problems cannot be fully resolved from eliminate small catchments and splitting large or long catchments into a uniform catchment size distribution but could certainly be improved. Ultimately, integrating cartographic, sensor, and model domain data will be an issue for all involved fields in the near future, and in some respects lay out the challenges for the next 20 years (Clarke et al, 2019).

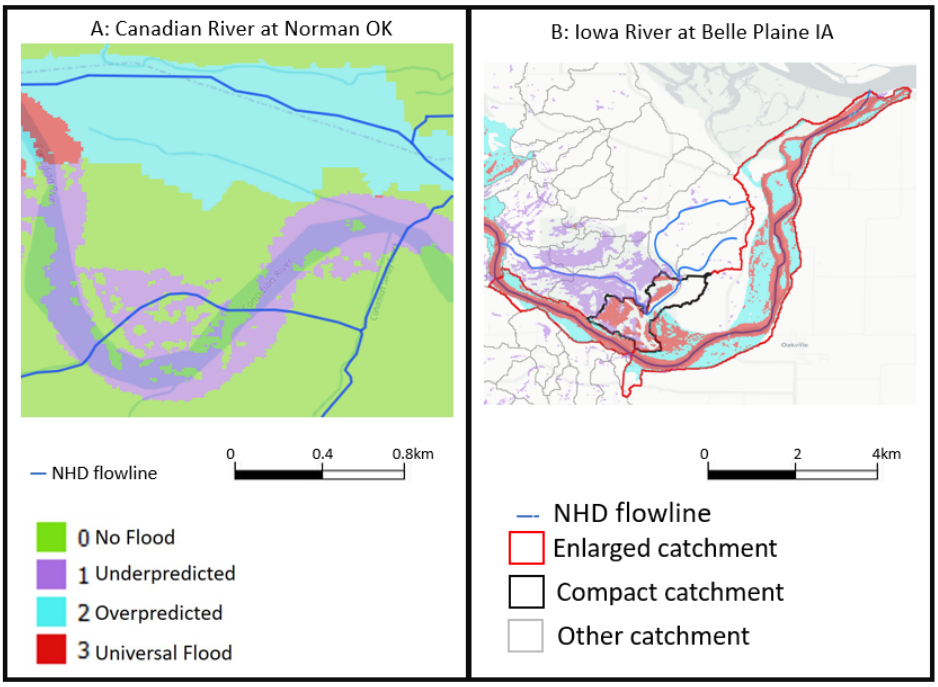

Figure 8: Unaccounted for challenges when using the NHD as a modelling fabric. (A) this catchment shows a case where the NHD/ NED is not capturing the true meander of a river channel (B) this set of catchments highlights the influence of long non-uniform catchments and challenges with catchment definition.

4.7 Remote sensing (RS) Challenges

In all analyses we treated the USFIMR maps as ground truth. For the sake of a robust comparison it is worth highlighting some of the issues that arise in the creation of remotely sensed inundation maps and their consequences in these comparisons.

4.7.1 Pixel misclassification

The spectral similarity of dark vegetation and water pixels in optical satellite imagery contributes to uncertainties in both directions. Most often, these errors resulted in isolated patches of dark vegetation being classified as water (Figure 9A FloodID 2). Other cases of pixel misclassification occurred in FloodIDs 1, 3, 16, 17, 18 and 23. Water was also incorrectly classified in a few notable cases. For example, pixels clearly within the main channel of the Mississippi river were classified as unflooded in Figure 9B (Flood ID 13). In this example, the NWM-HAND methodology correctly identified such locations as being flooded (despite over predicting the overall flood extent). These error types were also present in floods 19 and 23.

4.7.2 Image artefacts

Image artefacts also impact our comparison. The first is the well-known scan line error present in LANDSAT 7 images processed after 2003 (Scaramuzza and Barsi, 2005). Despite gap filling, some data gaps still remain. The gaps created by the scan line error (Figure 9C; Flood ID 4), created situations where both methods missed a flood or HAND-NWM alone predicts a flood, even though flooding could be detected from surrounding pixels. The overall extent covered by scan line gaps did not have a large impact as this issue affected only a relatively small percentage of the area in one case study.

The second artefact encountered was cloud cover which had a strong effect in one case study (Figure 9D; Flood ID 5). The image used to generate the USFIMR map was taken from a LANDSAT scene with 40% cloud cover, making it difficult to accurately classify some segments of the image. This comparison also contained large regions of freshly melted snow (visible in the LANDSAT image as well as from the road network and farm fields in the classified image). Cloud related classification errors also affected FloodID 15, but to a lesser degree.

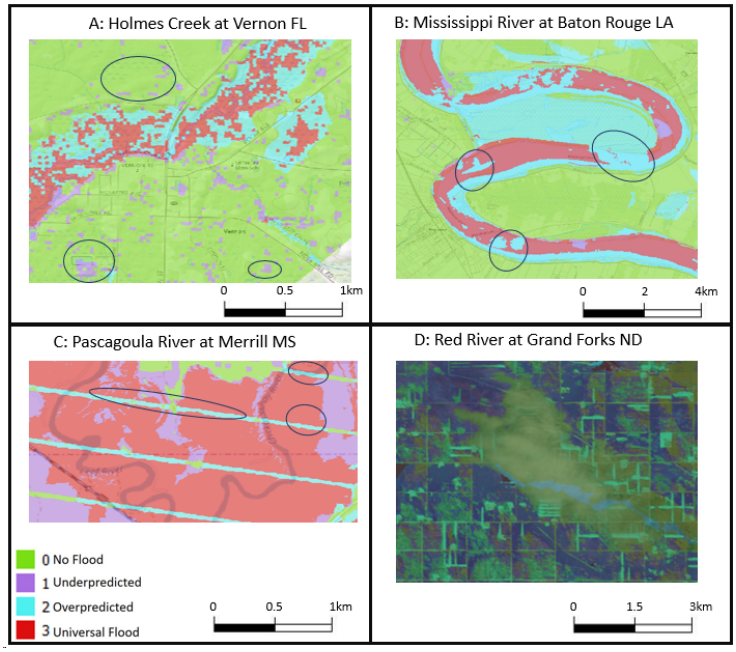

Fig 9: Errors due to classification issues and image artefacts: (A) Dark vegetation misclassified as water due to spectral similarity. (B) Misclassified channel segments due to spectral similarity. (C) Scan line errors in input RS image create gaps in flooded extent. (D) clouds and melted snow create ambiguities in flooded extent recognition.

In all cases, these errors only occurred in minor portions of a few floods used in the analysis. We raise them not because they adversely impacted our results but for transparency and to provide readers with an understanding that no form of ground-

truthing is infallible. The rigorous development, successful use in other studies, and our careful evaluation of each flood extent give us confidence in their overall accuracy. More importantly, such a resource is the only available option for validating modelled inundation extents at the scales we are exploring. As the NWM-HAND method continues to improve, be developed, and further validated, resources like the USFIMR will only become more necessary.

5. Discussion

At the floodplain resolution, NWM-HAND is able to accurately capture 10 - 27% of inundation (IQR) with a larger tendency to under (37 - 63%) then over predict (10 - 36%). To better understand how model performance is driven by NWM, we grouped a sample of 54 gaged catchments by relative NWM performance and found the NWM-HAND method is relatively insensitive to biases in NWM streamflow prediction accuracy - losing less than 10% relative accuracy. However, when the normalized mean error between observed and NWM predicted streamflow exceeds 60% the bias in inundation prediction is increased considerably. Overall, 66.7% of the catchments in our sample exhibited a NWM prediction accuracy with a nMAE less than 60%. In this paper we used a reanalysis product which was created with limited calibration and no data assimilation. When the NWM-HAND is used operationally, much of the data will come from the analysis and assimilation configuration which assimilates NWIS gage data and has had a more robust calibration. In theory this should allow a greater percent of reaches to fall within the 60% nMAE threshold.

In addition to errors in streamflow magnitude, NWM timing errors can introduce issues related to flood inundation forecasting and its evolution. Even though we did not explicitly study the ability of NWM-HAND to capture the temporal evolution of flood extents in this study, a few instances where the NWM improperly estimated the receding limb of the hydrograph, showed the inability of NWM-HAND to capture ponded and receding waters leading to issues of under and over prediction respectively.

We saw a larger tendency to overpredict (17% - 63% NWM) then underpredict (4 - 53%) inundation at the catchment level - the opposite pattern seen at the resolution of the floodplain. We argue that the tendency to underpredict area at the floodplain resolution was an aggregate result of consistently underpredicting many, small lower order catchments. From this we concluded that the base assumptions in the SRC generation was not adequately capturing lower order streams. Based on our tests, we found the SRCs are highly sensitive to the roughness coefficient used and insensitive to changes in floodplain cross-section. As a general rule we believe the default Manning's coefficient used by HAND is too small in low order reaches and are arguably too high in higher order reaches. While we only tested this on the small sample of available catchments, the theory behind the Manning values, and the consistent propensity to under predict low order reaches would support such a change. Moreover, in all of our tests the existing cross-sections geometries could be altered to provide correct Q when varying

Manning's n within a range of 0.0001 and 0.2. This leads us to suggest that further work with respect to the Manning's n values used should be prioritized

Another reoccurring error in our simulations was over prediction in catchments with low relief. Such catchments allow incremental changes in stage to have large impacts on inundation extent. We suggest that a refactoring of the NHD to smaller more uniform units, and a consideration for how volume rather than stage may be used to fill catchments, may be possible solutions. Moreover, the former offers some solutions to issues arising from treating the cartographic NHD as a modelling infrastructure. That said, neither of these are trivial to accomplish or validate.

While the overall NWM-HAND methods certainly have a long way to go, we contend the results demonstrate that the NWM-HAND approach of generating flood inundation maps is useful for general guidance and risk identification but may not be suitable for pixel level analysis, resource allocation, or risk-communication.

Despite the limited accuracy found in this study, the NWM-HAND is quite an achievement that should not be discounted. The fact that an uncalibrated continental-scale model can be used to rapidly generate flood inundation maps for all case studies with a single framework (code) is of great value. More importantly, the base layers and conceptual framework underpinning the model offer the research community a resource to improve, modify, and manipulate.

Looking towards future research and development; the inevitable next version of the base layers; and operational use, issues of availability arise. Currently, accessing and combining the needed NWM-HAND products is cumbersome, and for regions straddling one or more HUC6 can be data and processing intensive. While services like the Flood Mapping R package can streamline some of the steps, disseminating data by HUC6 is not a convenient choice for users. Instead HAND products could be distributed via a web service like those used to distribute climate data and NWM gridded output or built into services like the CUAHSI sub setter (CUASHI, 2019). With workable foundations now in place, engaging with the communities that will use these products for research, map creation, and ultimately in the field seems like a next step worth considering.

6. Conclusion

This study offers a high-level evaluation of the confidence we can place in the operational NWM-HAND forecasts. In its current state the NWM-HAND methods have limited ability to accurately capture inundation and its skill is more constrained by the terrain and SRC inputs then NWM accuracy.

At floodplain level, NWM-HAND tends to underestimate flooding (82% of case studies). Of these, the mean likelihood of underpredicting a missed cell (53%) is twice that of overprediction (27%). At the catchment scale, NWM-HAND was better able to capture the total area of inundation (improvement of a mean of 6% in comparison to the floodplain level) but was more likely to overpredict (44%) than underpredict (31%) missed cells. We attribute this disparity to systemic underprediction in lower order reaches. An analysis of NWM-HANDs sensitivity to changes in Manning's n and cross-sectional geometries indicate that SRCs are insensitive to changes in hydraulic radius (ergo wetted perimeters) but are very sensitive to changes in Manning's n. As a general rule of thumb, the current SRCs underpredict n in lower order reaches and overpredict n in higher order reaches. In all cross-sectional geometries we tested, observed streamflow (NWIS) stage (USFIMR cross section) relationships were achievable with a variable n, save those with zero relief.

We further investigated the level of bias in NWM-HAND maps coming from the NWM forecasts and found the method to be relatively insensitive until the normalized absolute error between NWM and observed flow exceeded 60%. Above this threshold, predictable patterns of large under or over prediction occur in the direction of the NWM miss.

Lastly, over prediction in large catchments with low relief is a common error. Aside from integrating higher resolution terrain data, two possible solutions for remedying these systemic errors include refactoring the catchment areas used to more uniform and compacts units, and a consideration of how NWM cross-sectional area forecasts (Streamflow / Velocity) can be used to better control the spread of water in areas of low relief.

While the current ability to capture accurate inundation is limited, our analysis revealed no fundamental errors that would render NWM-HAND unusable. Instead, we found that with modifications, accurate inundation is generally achievable at the level needed for guidance and emergency management. Therefore, we end with great optimism that further development, research and evaluation around the NWM-HAND method can deliver on its promise of a CONUS scale flood modelling enterprise.

Acknowledgements: We would like to thank David Tarboton and David Blodgett for their constructive reviews that helped shape this paper. USFIMR is funded through the NOAA National Water Center (NWC) via the UCAR COMET Program (2016/17), AOI, HydroData, and Flood Mapping R packages were developed through the NOAA National Water Center (NWC) and UCAR COMET Program (2017/18).

References

1. Afshari, S., Tavakoly, A.A., Rajib, M.A., Zheng, X., Follum, M.L., Omranian, E., Fekete, B.M., 2018. Comparison of new generation low-complexity flood inundation mapping tools with a hydrodynamic model. Journal of Hydrology 556, 539–556.

2. Blodgett, D., 2018. nhdplusTools, Github Repository. GitHub. github.com/dblodgett-usgs/nhdplusTools
3. Clarke, K. C., Johnson, J. M., & Trainor, T. (2019). Contemporary American cartographic research: a review and prospective. Cartography and Geographic Information Science, 46(3), 196-209.
4. Cline, D., Maidment, D., n.d. Community Advisory Committee for Water Prediction (CAC-WP).
5. Cohen, S., Brakenridge, G. R., Kettner, A., Bates, B., Nelson, J., McDonald, R., Huang, Y., Munasinghe, D., Zhang, J. (2018). Estimating floodwater depths from flood inundation maps and topography. JAWRA Journal of the American Water Resources Association, 54(4), 847-858.
6. CUASHI, 2019. NWM-Subsetting. Github Repository. Github.https://github.com/CUAHSI/nwm_subsetting
7. FEMA, 2007. National Elevation Dataset (NED) and similar USGS Holdings. https://hazards.fema.gov/femaportal/docs/National%20Elevation%20Dataset_2007.pdf
8. Gochis, D., Dugger, A., McCreight, J., Karsten, L.R., Logan, Yu, W., Pan, L., Yates, D., Zhang, Y., Sampson, K., Cosgrove, B., Salas, F., Clark, E., Graziano, T., Maidment, D., Phan, C., Cui, Z., Liu, Y., Feng, X., Lee, H., 2016. Technical Description of the National Water Model Implementation of WRF-Hydro, CUAHSI Technical Report.
9. Gochis, D.J., Dugger, A., Barlage, M., Fitzgerald, K., Karsten, L., McAllister, M., McCreight, J., Mills, J., Rafieeinasab, A., Read, L., Sampson, K., Yates, D., Yu, W., 2018. The NCAR WRF-Hydro Modeling System Technical Description [WWW Document]. ral.ucar.edu. URL https://ral.ucar.edu/sites/default/files/public/WRF-HydroV5TechnicalDescription.pdf (accessed 8.21.18).
10. Henstra, D., Minano, A., Thistlethwaite, J., 2019. Communicating disaster risk? An evaluation of the availability and quality of flood maps. Natural Hazards and Earth System Sciences 19, 313–323.
11. Hirabayashi, Y., Mahendran, R., Koirala, S., Konoshima, L., Yamazaki, D., Watanabe, S., Kim, H., Kanae, S., 2013. Global flood risk under climate change. Nature Publishing Group 3, 816.
12. Johnson, J.M., 2019a. AOI, Github Repository. doi:https://doi.org/10.5281/zenodo. .1318687
13. Johnson, J.M., 2019b. Flood Mapping, Github Repository. doi:https://doi.org/10.5281/zenodo.2588009
14. Johnson, J.M., 2018a. NWM, Github Repository. GitHub. doi:10.5281/zenodo.1401394
15. Johnson, J.M., 2018b. HydroData. doi:10.5281/zenodo.1401393
16. Johnson, J.M., Cole, J.M., 2017. National Water Center Innovators Programs Summer Institute Report 2017. doi:10.4211/technical.20171009
17. Johnson, J.M., Coll, J.M., Ruess, P.J., Hastings, J.T., 2018. Challenges and Opportunities for Creating Intelligent Hazard Alerts: The “FloodHippo” Prototype. Journal of the American Water Resources Association.
18. Johnson, J.M., Ruess, P., & Coll, J. (2016). OPERA–Operational Platform for Emergency Response and Awareness: Reimagining Disaster Alerts. National water center innovators program summer institute report 2016, 4, 97.
19. Lam, L., 2018. A Concerning Trend: Flooding Deaths Have Increased in the U.S. the Last Few Years | The Weather Channel.
20. Lightbody, L., Tompkins, F., 2018. Where It Rains, It Floods.
21. Li, Z., 2016. A Framework of ArcGIS-Based Flood Inundation Modeling and Mapping System. ESRI Proceedings. http://proceedings.esri.com/library/userconf/proc16/papers/265_671.pdf
22. Liu, Y.Y., Maidment, D.R., Tarboton, D.G., Zheng, X., Wang, S., 2018. A CyberGIS Integration and Computation Framework for High-Resolution Continental-Scale Flood Inundation Mapping. Journal of the American Water Resources Association.
23. Maidment, D.R., 2016. Conceptual Framework for the National Flood Interoperability Experiment. J Am Water Resour Assoc 53, 245–257. doi:10.1111/1752-1688.12474

24. Maidment, D.R., 2009. FEMA flood map accuracy: Presented at the World Environmental and Water Resources Congress 2009: Great Rivers, pp. 1–10.
25. Merz, B., Thieken, A.H., Gocht, M., 2007. Flood risk mapping at the local scale: concepts and challenges, in: Flood Risk Management in Europe. Springer, pp. 231–251.
26. Munasinghe, D., Cohen, S., Huang, Y.F., Tsang, Y.P., Zhang, J., Fang, Z., 2018. Intercomparison of Satellite Remote Sensing-Based Flood Inundation Mapping Techniques. JAWRA Journal of the American Water Resources Association, 54(4), 834-846.
27. National Research Council, 2009. Mapping the zone: Improving flood map accuracy. National Academies Press.
28. NOAA, 2016a. National Water Model [WWW Document]. httpwater.noaa.govdocumentswrn-national-water-model.pdf. URL http://water.noaa.gov/documents/wrn-national-water-model.pdf (accessed 8.21.18a).
29. NOAA, 2016b. Experimental Water Information Interface Webpage Product Description Document [WWW Document]. water.noaa.gov. URL http://water.noaa.gov/documents/OWP-interface-PDD.pdf (accessed 8.21.18b).
30. NOAA National Water Center, E. Boghici, D. Arctur (2018). NOAA NWC - Harvey NWM-HAND Flood Extents, HydroShare, https://doi.org/10.4211/hs.fe85a680d0144e79b39e8c483dc1e5aa
31. Rennó, C.D., Nobre, A.D., Cuartas, L.A., Soares, J.V., Hodnett, M.G., Tomasella, J., Waterloo, M.J., 2008. HAND, a new terrain descriptor using SRTM-DEM: Mapping terra-firme rainforest environments in Amazonia. Remote Sensing of Environment 112, 3469–3481.
32. Rodda, H.J., 2005. The development and application of a flood risk model for the Czech Republic. Natural hazards 36, 207–220.
33. Ross, N., 2018 fasterize: Fast Polygon to Raster Conversion. R package version 1.0.0. https://CRAN.R-project.org/package=fasterize
34. Salas, F.R., Somos-Valenzuela, M.A., Dugger, A., Maidment, D.R., Gochis, D.J., David, C.H., Yu, W., Ding, D., Clark, E.P., Noman, N., 2017. Towards Real-Time Continental Scale Streamflow Simulation in Continuous and Discrete Space. J Am Water Resour Assoc 51, 10078–21. doi:10.1111/1752-1688.12586
35. Scaramuzza, P., Barsi, J., 2005. Landsat 7 scan line corrector-off gap-filled product development, in:. Presented at the Proceeding of Pecora, pp. 23–27.
36. Sangwan, N., & Merwade, V.,2015. A faster and economical approach to floodplain mapping using soil information. JAWRA Journal of the American Water Resources Association, 51(5), 1286-1304.
37. Tesfa, T. K., Tarboton, D. G., Watson, D. W., Schreuders, K. A., Baker, M. E., & Wallace, R. M. (2011). Extraction of hydrological proximity measures from DEMs using parallel processing. Environmental Modelling & Software, 26(12), 1696-1709.
38. Yin, J., Gentine, P., Zhou, S., Sullivan, S.C., Wang, R., Zhang, Y., Guo, S., 2018. Large increase in global storm runoff extremes driven by climate and anthropogenic changes. Nature Communications 9, 4389.
39. Zheng, X., Maidment, D.R., Tarboton, D.G., Liu, Y.Y., Passalacqua, P., 2018. GeoFlood: Large-Scale Flood Inundation Mapping Based on High-Resolution Terrain Analysis. Water Resour. Res.
40. Zheng, X., Tarboton, D.G., Maidment, D.R., Liu, Y.Y., Passalacqua, P., 2017. River channel geometry and rating curve estimation using height above the nearest drainage. Journal of the American Water Resources Association.

8. APPENDIX

Table 1. Flood events used for comparison

FloodID	River name	Flood date	Satellite sensor	State	Flood area (km^2)
1	Choctawhatchee River	4-Jan-16	Landsat 8 OLI	FL	1493
2	Holmes Creek	4-Jan-16	Landsat 8 OLI	FL	129
3	Pea River	4-Jan-16	Landsat 8 OLI	AL	407
4	Pascagoula River	17-Mar-11	Landsat 7 ETM+	MS	1692
5	Red River	18-Apr-97	Landsat 5 TM	ND	7777
6	Brazos River	28-May-16	Landsat 8 OLI	TX	74
7	Spring Creek	28-May-16	Landsat 8 OLI	TX	160
8	Willow Creek	28-May-16	Landsat 8 OLI	TX	48
9	Washita River	29-May-15	Sentinel-1 VH Polarization	OK	623
10	Brazos River	30-May-16	Sentinel-1 HV Polarization	TX	951
11	San Jacinto River	30-May-16	Sentinel-1 HV Polarization	TX	212
12	Canadian River	17-Jun-15	Sentinel-1 VH Polarization	OK	739
14	Trempealeau River	26-Sep-10	Landsat 5 TM	WI	276
15	Wisconsin River	26-Sep-10	Landsat 5 TM	WI	8350
17	Iowa River	26-Sep-16	Landsat 8 OLI	IA	3541
18	Maquoketa River	26-Sep-16	Landsat 8 OLI	IA	2249
19	Mississippi River	26-Sep-16	Landsat 8 OLI	IA	1937
20	Wapsipinicon River	26-Sep-16	Landsat 8 OLI	IA	4148
21	Minnesota River	1-Oct-10	Landsat 5 TM	MN	7876
22	Redwood River	1-Oct-10	Landsat 5 TM	MN	1414
23	Mississippi River	3-Oct-10	Landsat 5 TM	MN	6957
24	Ashley River	13-Oct-16	Landsat 8 OLI	SC	1804
25	Black River	13-Oct-16	Landsat 8 OLI	SC	431
26	Cooper River	13-Oct-16	Landsat 8 OLI	SC	2096
27	Lumber River	13-Oct-16	Landsat 8 OLI	SC, NC	1116
28	Neuse River	15-Oct-16	Landsat 8 OLI	NC	1054
29	Tar River	15-Oct-16	Landsat 8 OLI	NC	1702
30	Rio Grande River	14-Jul-10	Landsat 7 ETM+	TX	6836